Light Scattering from Collision-Dominated Plasmas*†

E. M. Leonard and R. K. Osborn
Department of Nuclear Engineering, The University of Michigan, Ann Arbor, Michigan 48105
(Received 21 March 1973)

The scattering of electromagnetic radiation by a fully ionized, collision-dominated plasma in a magnetic field is investigated using a stochastic approach. The stochastic equations for the density-fluctuation operators are modified to include particle collisions through a Bhatnagar-Gross-Krook collision model. The equations of this model are constructed to conserve particle number, energy, and momentum. Explicit numerical results are obtained in the absence of magnetic fields and compared to experimental values and other theories. The analytical results are assumed valid for plasmas which can be characterized by Maxwellian velocity distributions for electrons and ions at the same or different temperatures.

I. INTRODUCTION

The problem of light scattering from a fully ionized plasma has been investigated from a number of different viewpoints.[1-7] To our knowledge no one has used a Bhatnagar-Gross-Krook[8] (BGK) collision model which conserves particle number, energy, and momentum to describe charged-particle binary collisions in the light-scattering problem. Use has been made of this model in the description of collisions in fluids[9] and charged-particle–neutral collisions in plasmas.[10,11] Here we apply this model, which may (at least in part) account for binary collisions between charged particles, to a fully ionized plasma in a magnetic field. Collisions between unlike particles are not included in this analysis.

We use a stochastic approach to the calculation of the spectrum of electromagnetic radiation scattered from a plasma along with a BGK model to describe collisions. In the limit of no collisions our results reduce to those of Salpeter[1,2] both with and without magnetic fields. The calculated spectra in the collisionless case are in agreement with the numerical results of Williamson, Nodwell, and Barnard.[12] When collisions are included, the results agree qualitatively with those of DuBois and Gilinsky[3] for the shape of the central peak. The expected effect of collisions on the resonance at the plasma frequency is also obtained.[1] This model allows an analytic solution from which numerical results are relatively easily obtained.

In Sec. II we introduce the model and present the formulism necessary for the calculation of the scattering function. The explicit solution is obtained for the scattering cross section. Results of numerical calculations are shown in Sec. III and compared with experiments and other theories. In Sec. IV we briefly comment on our results.

II. FORMULATION

The cross section for the scattering of electromagnetic radiation from a plasma is given by

$$\sigma = (\omega'/\omega'')\,\sigma_T S(\vec{k},\omega), \tag{1}$$

where σ_T is the differential Thomson cross section and ω'' and ω' are the angular frequencies of the incoming and scattered radiation, respectively. The quantity $S(\vec{k},\omega)$ is the scattering function, where $\omega=\omega''-\omega'$ and $\vec{k}=\vec{k}''-\vec{k}'$, i.e.,

$$S(\vec{k},\omega) = (2\pi n_e)^{-1}\int dt\, e^{-i\omega t}\int d\vec{r}\,d\vec{r}\,'\,d\vec{v}\,d\vec{v}\,'\,e^{i\vec{k}\cdot(\vec{r}-\vec{r}\,')} \times\langle \delta f^e{}^*(\vec{r}\,',\vec{v}\,',0)\,\delta f^e(\vec{r},\vec{v},t)\rangle . \tag{2}$$

The quantity δf^e is the electron-density fluctuation operator defined in the Appendix, n_e is the number of electrons in the scattering volume, and the angular brackets represent an average over an appropriate probability distribution. The remainder of this section is devoted to the calculation of the function defined in Eq. (2).

As a starting point we consider the linearized equations for the density fluctuations in a fully ionized plasma in an external magnetic field, i.e.,

$$\frac{\partial}{\partial t}\delta f^j(\vec{r},\vec{v},t)+\vec{v}\cdot\frac{\partial \delta f^j}{\partial \vec{r}}+\frac{q^j}{m_j c}(\vec{v}\times\vec{B})\cdot\frac{\partial \delta f^j}{\partial \vec{v}}-\frac{N_j}{m_j}\frac{\partial f_0^j}{\partial \vec{v}}\cdot\int d\vec{r}\,'d\vec{v}\,'\,\frac{\partial V^{jj}}{\partial \vec{r}}\,\delta f^j(\vec{r}\,',\vec{v}\,',t)$$
$$-\frac{N_j}{m_j}\frac{\partial f_0^j}{\partial \vec{v}}\cdot\int d\vec{r}\,'d\vec{v}\,'\,\frac{\partial V^{jk}}{\partial \vec{r}}\,\delta f^k(\vec{r}\,',\vec{v}\,',t)$$
$$-I^{jj}\delta f^j - I^{kj}\delta f^j - I^{jk}\delta f^k = \mathcal{S}^j(\vec{r},\vec{v},t), \tag{3}$$

where $\mathcal{S}^j(\vec{r},\vec{v},t)$ is a stochastic function[13,14] and f_0^j is chosen to be a Maxwellian velocity distribution for the jth species. The quantity N_j is the particle-number density. The collision integrals (see Appendix) will be carried along in a symbolic fashion until approximations become necessary.

Taking the Fourier transform of Eq. (3) and rewriting it in matrix form, one obtains

$$\frac{\partial}{\partial t}\Psi(\vec{k},\vec{v},t)+M\Psi=\mathcal{S}(\vec{k},\vec{v},t), \tag{4}$$

where

$$\Psi(\vec{k},\vec{v},t)=\begin{bmatrix}\delta f^e(\vec{k},\vec{v},t)\\ \delta f^i(\vec{k},\vec{v},t)\end{bmatrix},$$

$$\mathcal{S}(\vec{k},\vec{v},t)=\begin{bmatrix}\mathcal{S}^e(\vec{k},\vec{v},t)\\ \mathcal{S}^i(\vec{k},\vec{v},t)\end{bmatrix},$$

and

$$M=\begin{bmatrix}M_{11} & M_{12}\\ M_{21} & M_{22}\end{bmatrix}.$$

The matrix elements of M are

$$M_{11}=-i\vec{k}\cdot\vec{v}+\omega_{ce}(\vec{v}\times\hat{B})\cdot\frac{\partial}{\partial\vec{v}}+iU^{ee}\int d\vec{v}'-I^{ee}-I^{ie},$$

$$M_{12}=iU^{ei}\int d\vec{v}'-I^{ei},$$

$$M_{21}=M_{12}(e\rightleftarrows i),$$

and

$$M_{22}=M_{11}(e\rightleftarrows i),$$

where

$$U^{jk}=\frac{N_j}{m_j}V^{jk}(\vec{k})\vec{k}\cdot\frac{\partial}{\partial\vec{v}}f_0^j,$$

and

$$\omega_{cj}=q_jB/m_jc.$$

Next we define a correlation matrix as[14]

$$\Lambda(\vec{k},\vec{v}',\vec{v},\omega)\equiv\langle\Psi^*(\vec{k},\vec{v}',\omega)\tilde{\Psi}(\vec{k},\vec{v},\omega)\rangle, \tag{5}$$

where $\tilde{\Psi}$ is the transpose of Ψ. Taking the Fourier transform in time of Eq. (4) and solving for $\Psi(\vec{k},\vec{v},\omega)$ one obtains

$$\Lambda=[-i\omega I+M^*(\vec{k},\vec{v}')]^{-1}D(\vec{k},\vec{v}',\vec{v})[i\omega I+\tilde{M}(\vec{k},\vec{v})]^{-1}, \tag{6}$$

where we have used, as a first approximation, the assumption that[13]

$$\langle\mathcal{S}^*(\vec{k},\vec{v},t)\tilde{\mathcal{S}}(\vec{k},\vec{v}',t')\rangle\simeq\delta(t-t')D(\vec{k},\vec{v},\vec{v}'). \tag{7}$$

It can be shown that[14]

$$D(\vec{k},\vec{v}',\vec{v})=M^*(\vec{k},\vec{v}')\Omega(\vec{k},\vec{v}',\vec{v})+\Omega(\vec{k},\vec{v}',\vec{v})\tilde{M}(\vec{k},\vec{v}),$$

where

$$\Omega(\vec{k},\vec{v}',\vec{v})\equiv\langle\Psi^*(\vec{k},\vec{v}',t'=0)\tilde{\Psi}(\vec{k},\vec{v},t=0)\rangle.$$

For the equilibrium case the approximate values of the matrix elements $\Omega(\vec{k},\vec{v}',\vec{v})$ are known.[15] Using the above expressions and defining

$$\Lambda(\vec{k},\omega)\equiv\int d\vec{v}\,d\vec{v}'\Lambda(\vec{k},\vec{v}',\vec{v},\omega), \tag{8}$$

one obtains, for the correlation matrix,

$$\Lambda(\vec{k},\omega)=2\,\mathrm{Re}\int d\vec{v}\,d\vec{v}'[M(\vec{k},\vec{v})+i\omega I]^{-1}\Omega(\vec{k},\vec{v}',\vec{v}). \tag{9}$$

We define a new function

$$G(\vec{k},\vec{v},\omega)\equiv\int d\vec{v}'[M(\vec{k},\vec{v})+i\omega I]^{-1}\Omega(\vec{k},\vec{v},\vec{v}'). \tag{10}$$

The scattering function is now obtained in terms of the electron-density fluctuations, i.e.,

$$S(\vec{k},\omega)=(2\pi n_e)^{-1}\Lambda_{11}(\vec{k},\omega), \tag{11}$$

where

$$\Lambda_{11}(\vec{k},\omega)=2\,\mathrm{Re}\int d\vec{v}\,G_{11}(\vec{k},\vec{v},\omega). \tag{12}$$

In order to solve for G_{11} we note that $G(\vec{k},\vec{v},\omega)$ is actually a 2×2 matrix, and that Eq. (10) can be written as two coupled pairs of equations. The coupled pair of interest is

$$(i\omega+M_{11})G_{11}+M_{12}G_{21}=\int d\vec{v}'\,\Omega_{11}(\vec{k},\vec{v},\vec{v}')$$

and

$$(i\omega+M_{22})G_{21}+M_{21}G_{11}=\int d\vec{v}'\,\Omega_{21}(\vec{k},\vec{v},\vec{v}'), \tag{13}$$

where the matrix elements M are the same as those in Eq. (4).

We transform Eqs. (13) back into the real space and time domain and arrive at expressions for $G_{11}(\vec{r},\vec{v},t)$ and $G_{21}(\vec{r},\vec{v},t)$ which are similar to Eq. (3) with the stochastic functions $\mathcal{S}^e$ and $\mathcal{S}^i$ replaced by the known quantities Ω_{11} and Ω_{21}.

To proceed further it becomes necessary to specify the collision operators. We will neglect the cross-collision terms and represent the self-collisions by a BGK collision model[8]

$$I^{ee}G_{11}=\left[-\nu_{ee}+\nu_{ee}f_0^e\int d\vec{v}+\nu_{ee}f_0^e\frac{2\vec{v}}{v_e^2}\int\vec{v}\,d\vec{v}+\nu_{ee}f_0^e\left(\frac{v^2}{v_e^2}-\frac{3}{2}\right)\frac{1}{v_e^2}\int v^2\,d\vec{v}-\nu_{ee}f_0^e\left(\frac{v^2}{v_e^2}-\frac{3}{2}\right)\int d\vec{v}\right]G_{11}(\vec{r},\vec{v},t). \tag{14}$$

A similar expression is obtained for $I^{ii}G_{21}$. The term ν_{jj} is a velocity-independent collision frequency of the jth species, and $v_j^2 = 2\Theta_j/m_j$, where Θ_j is the temperature in energy units.

The equations for G_{11} and G_{21} are now solved to obtain

$$G_{11}(\vec{k},\vec{v},\omega) = \sum_{n=-\infty}^{+\infty}\sum_{m=-\infty}^{+\infty} \frac{J_n(k_1 v_\perp/|\omega_{ce}|)J_m(k_1 v_\perp/|\omega_{ce}|)}{\nu_{ee} + i\omega - ik_3 v_3 - im\omega_{ce}} \times e^{i\varphi(n-m)} \left\{ i\left(\frac{N_e}{\Theta_e}\right) f_0^e [V^{ee}(\vec{k})\eta^e(\vec{k},\omega) + V^{ei}(\vec{k})\eta^i(\vec{k},\omega)](m\omega_{ce} + k_3 v_3) + \nu_{ee} f_0^e \left[\eta^e(\vec{k},\omega) + \left(\frac{2N_e}{v_e^2}\right)\vec{v}\cdot\vec{q}^e(\vec{k},\omega) + \frac{N_e}{\Theta_e}\left(\frac{v^2}{v_e^2} - \frac{3}{2}\right)\tau^e(\vec{k},\omega)\right] + N_e f_0^e (1 - C_k)\right\} \quad (15a)$$

and

$$G_{21}(\vec{k},\vec{v},\omega) = \sum_{n=-\infty}^{+\infty}\sum_{m=-\infty}^{+\infty} \frac{J_n(k_1 v_\perp/\omega_{ci})J_m(k_1 v_\perp/\omega_{ci})}{\nu_{ii} + i\omega - ik_3 v_3 - im\omega_{ci}} \times e^{-i\varphi(n-m)} \left\{ i\left(\frac{N_i}{\Theta_i}\right) f_0^i [V^{ii}(\vec{k})\eta^i(\vec{k},\omega) + V^{ie}(\vec{k})\eta^e(\vec{k},\omega)](m\omega_{ci} + k_3 v_3) + \nu_{ii} f_0^i \left[\eta^i(\vec{k},\omega) + \left(\frac{2N_i}{v_i^2}\right)\vec{v}\cdot\vec{q}^i(\vec{k},\omega) + \frac{N_i}{\Theta_i}\left(\frac{v^2}{v_i^2} - \frac{3}{2}\right)\tau^i(\vec{k},\omega)\right] + N_e C_k f_0^i \right\}, \quad (15b)$$

where

$$\int G_{11}(\vec{k},\vec{v},\omega)\,d\vec{v} \equiv \eta^e(\vec{k},\omega),$$

$$\int \vec{v} G_{11}(\vec{k},\vec{v},\omega)\,d\vec{v} \equiv N_e \vec{q}^e(\vec{k},\omega), \quad (16)$$

and

$$\int v^2 G_{11}\,d\vec{v} \equiv \frac{3v_e^2 N_e}{2\Theta_e}\tau^e(\vec{k},\omega) + \tfrac{3}{2}v_e^2\eta^e(\vec{k},\omega).$$

Expressions similar to Eqs. (16) with electron terms replaced by ion terms are obtained for G_{21}. The functions $J_n(y)$ are Bessel functions and[15]

$$C_k = [(1+Z)(1+k^2\lambda_D^2)]^{-1}, \quad (17)$$

where Z is the charge on the ion. We take the Debye length λ_D to be

$$\lambda_D \equiv \left(\frac{\Theta_e\Theta_i}{4\pi N_e e^2(\Theta_i + Z\Theta_e)}\right)^{1/2}. \quad (18)$$

The magnetic field is taken in the 3 direction, the wave vector $\vec{k}$ is chosen in the 1-3 plane, and $v_\perp$ is the magnitude of the component of velocity perpendicular to the magnetic field.

Making use of Eqs. (15) along with the moments defined in Eqs. (16), we arrive at ten equations in ten unknowns. These equations may then be solved numerically for $\eta^e(\vec{k},\omega)$ to give the scattering function, since

$$S(\vec{k},\omega) = (\pi n_e)^{-1}\,\mathrm{Re}\,\eta^e(\vec{k},\omega). \quad (19)$$

In the absence of collisions these results reduce to those of Salpeter[1,2] both with and without a magnetic field. The remainder of this paper will deal with the special case of no external magnetic field in which we solve for $S(\vec{k},\omega)$ numerically. These results are discussed in Sec. III.

III. RESULTS

A. Preliminary Discussion

In this section we discuss the numerical results obtained by applying Eqs. (15) in the absence of magnetic fields to a number of specific cases. In formulating the problem we have assumed a fully ionized plasma with Maxwellian velocity distributions. The results presented are for hydrogen plasmas unless otherwise specified. The incident radiation is taken to be 6943-Å ruby laser light in most cases, and the scattering angle is specified. Both one- and two-temperature plasmas are considered. It was found that the energy-conserving term in the BGK approximation did not make any contribution to the shape of the scattered spectrum. The momentum-conserving term, on the other hand, has a significant effect in collision-dominated cases.

The spectrum of the scattered radiation is considered in two parts: (i) the central peak, where most of the scattered radiation is observed, and (ii) the satellite, or electron feature, which is located near the plasma frequency. We calculate these two parts of the scattered spectrum for a number of different plasmas using both a collisionless model and the collision model outlined in Sec. II. The effect of collisions is most pronounced for high-density low-temperature plasmas as expected.

We deal mainly with cases in which ion-electron collective effects are important, that is, the scattering wave vector $|\vec{k}| << (\lambda_{De})^{-1}$, where λ_{De} is the electron Debye length of the plasma. The wave vector is given by

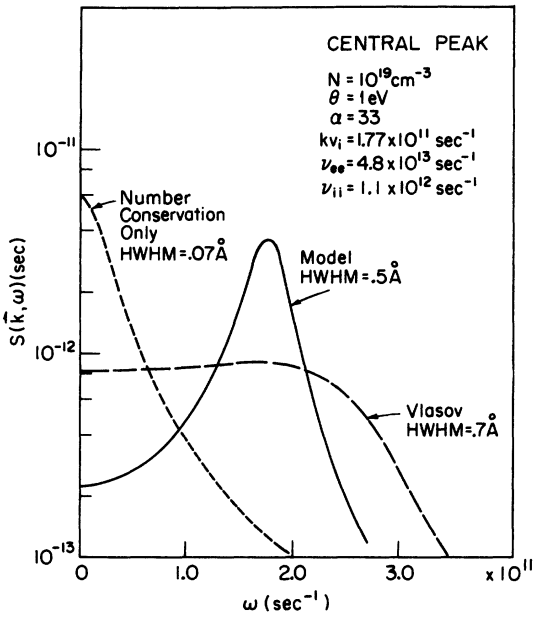

FIG. 1. Ion feature of the scattering function $S(\vec{k},\omega)$ as predicted by three different models. (HWHM = half-width at half-maximum).

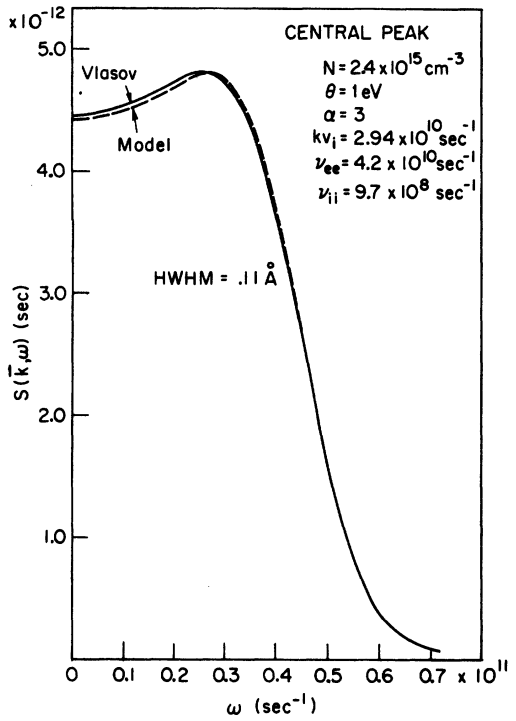

FIG. 2. Ion feature of the scattering function. The solid curve corresponds to the collisionless calculation, while the dashed line represents the BGK collision-model results.

$$\vec{k} = \vec{k}_{las} - \vec{k}_{scat} \tag{20}$$

and its magnitude is

$$|\vec{k}| = (4\pi/\lambda_{las}) \sin\tfrac{1}{2}\varphi, \tag{21}$$

where φ is the angle between the incident and scattered beams. The electron Debye length is given by

$$\lambda_{De} = (\Theta_e/4\pi N_e e^2)^{1/2}, \tag{22}$$

where Θ_e and N_e are the electron temperature and density, respectively.

A measure of the importance of these collective effects is given by the parameter α where

$$\alpha = (k\lambda_{De})^{-1}. \tag{23}$$

For $\alpha > 1$, interactions between electrons and ions bring about an ion-broadened central peak and cause plasma resonance peaks or satellites to appear in the neighborhood of the plasma frequency. For $\alpha < 1$ the scattered spectrum is determined by the Doppler broadening of the electron distribution. The collision frequencies are calculated in the manner described by Spitzer.[16]

B. Analysis of Results

1. *Central Peak*

For the case where $\alpha > 1$, interactions between electrons and ions produce a distinct feature centered about zero frequency as shown in Figs. 1 and 2. In Fig. 1 we consider a plasma with a density of 10^{19} cm^{-3}, a temperature of 1 eV, and $\alpha = 33$. The collisionless or Vlasov case has a slight dip in the center with peaks at approximately the ion-acoustic frequency kv_i. The collision model leads to a rather strong enhancement at the ion-acoustic frequency and a corresponding dip at the center. This is also predicted by DuBois and Gilinsky[3] for collision-dominated plasmas in which the acoustic frequency is less than either the electron-electron or ion-ion collision frequencies as is the case here. The remaining curve on Fig. 1 is the result obtained with our collision model when the momentum and energy-conserving terms are ignored. The results are in qualitative agreement with those obtained using a modified Fokker-Planck model which conserves only particle number.[4]

Collision frequencies are considerably lower in the case displayed in Fig. 2. As in Fig. 1, we are scattering 6943-Å ruby laser light from a 1-eV hydrogen plasma. In this case the plasma density is only 2.4×10^{15} cm^{-3}, which accounts for the lower collision frequencies. The fact that this line is a good deal narrower is a result of the lower ion-acoustic frequency which is due to a smaller momentum transfer of the scattered light. Whereas Fig. 1 deals with 90° scattering, Fig. 2 represents the observed scattered spectrum at

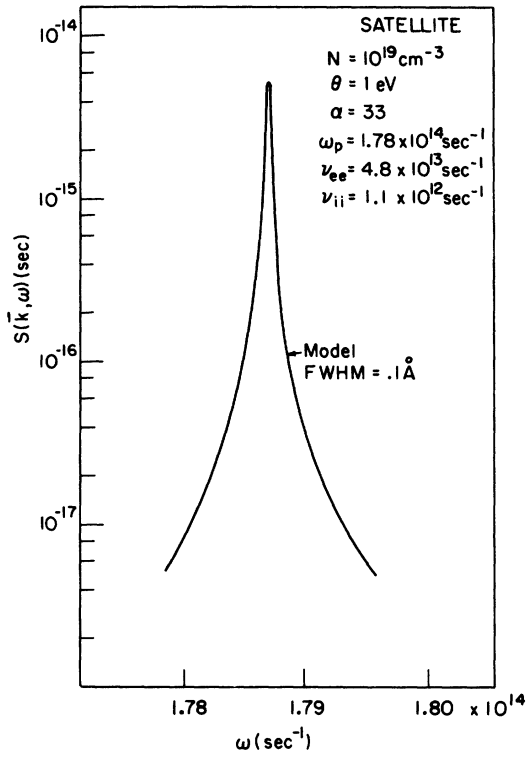

FIG. 3. Electron satellite peak of the scattering function calculated using the BGK collision model.

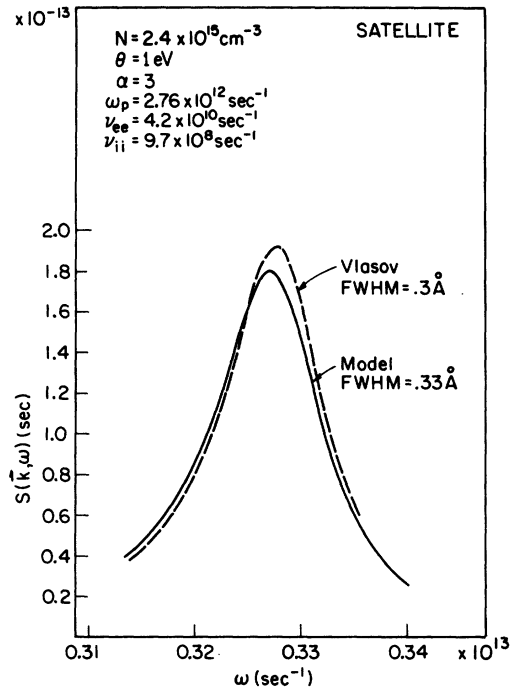

FIG. 4. Electron satellite peak of the scattering function. The BGK model is indicated by the solid curve while the collisionless case is represented by the dashed curve.

13.5°. The effect of collisions is small in this case, as one might expect, but it should be noted that collisions tend to make the acoustic peak more pronounced as in Fig. 1.

2. *Satellite*

In Fig. 3 we again consider the dense low-temperature plasma of Fig. 1—this time, though, we are looking in the region of the plasma frequency. Since Landau damping alone is not enough to broaden this resonance to the point where it can be resolved by this calculation, the collisionless case is not shown in the figure. It is seen that collisions significantly broaden the line in this case.

This is not the case in Fig. 4 in which a relatively low-collision-rate plasma is considered. Here the broadening due to collisions is rather insignificant. This might be expected since the effect of collisions on the central peak (Fig. 2) was also negligible.

The approximate position of the satellite is given by[17]

$$\omega_{\max} = (\omega_p^2 + 3\Theta_e k^2/m_e)^{1/2}, \tag{24}$$

which can also be written

$$\omega_{\max} = \omega_p(1 + 3/\alpha^2)^{1/2}. \tag{25}$$

We see that the larger the value of α, the less displacement of the satellite from ω_p. This is illustrated by Figs. 3 and 4.

3. CO_2 *Scattering*

The preceding discussion has been concerned entirely with the scattering of ruby laser (6943-Å) light from hydrogen plasmas. Figure 5 shows the spectrum, both with and without collisions, obtained when the CO_2 laser radiation (10.6 μ) is scattered from a hydrogen plasma with a density of 10^{18} cm^{-3} and a temperature of 1 eV. Qualitatively, the results are very much like those in Fig. 1. It is interesting to note that the half-widths in this case are an order of magnitude greater than those calculated for an incident radiation of 6943 Å. As CO_2 laser technology improves, this may be an aspect of laser diagnostics that could prove useful.

4. *Two-Temperature Plasmas*

The calculation of the scattering function is sufficiently general to allow consideration of electrons and ions at different temperatures. The first case we examine is illustrated in Fig. 6. Here the parameters are chosen to compare with Rosenbluth and Rostoker.[5] They examined the

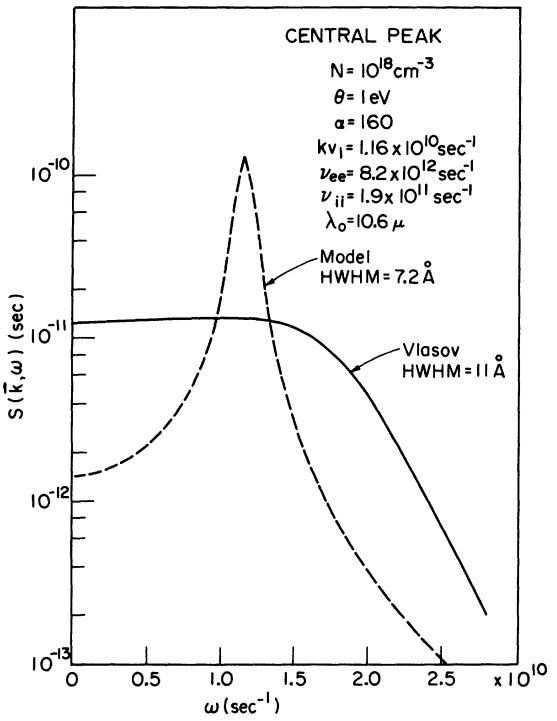

FIG. 5. Ion feature of the scattering function for 10.6 $-\mu$ radiation scattered from a hydrogen plasma.

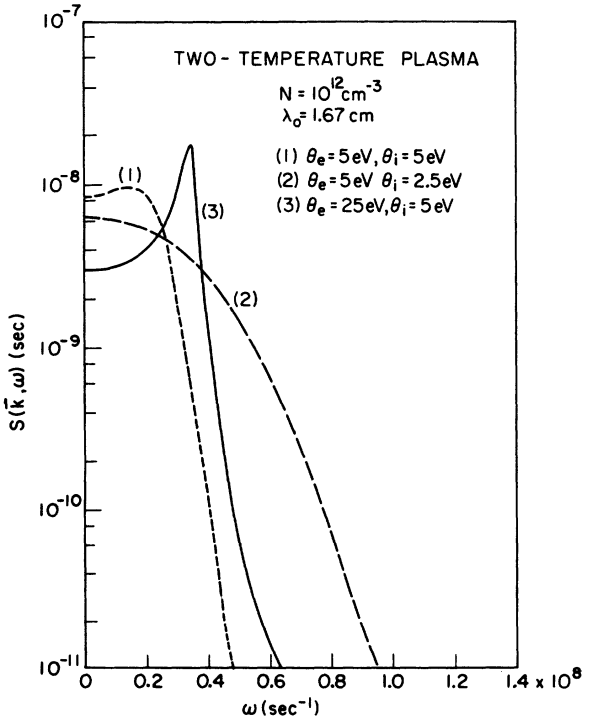

FIG. 6. Ion feature of the scattering function for a two-temperature plasma. Curve 1 represents a plasma in thermal equilibrium and curves 2 and 3 are for $\Theta_i > \Theta_e$ and $\Theta_e > \Theta_i$, respectively.

scattering of long-wavelength radiation (1.67 cm) from a low-density (10^{12}-cm^{-3}) hydrogen plasma.

Curve 1 is the characteristic central peak obtained for a plasma in thermal equilibrium. The case in which $\Theta_i > \Theta_e$ is illustrated in curve 2 and can be interpreted as Doppler broadening due to the ion thermal velocity. When $\Theta_e > \Theta_i$, curve 3 is obtained. All three curves are in agreement with Ref. 5.

Although our aim has been to investigate high-density low-temperature plasmas in which collisions have some effect, the above calculation is given as a means of gaining more confidence in our results. At this point we consider the scattered spectrum for two-temperature plasmas in which collisions may play a role in the determination of the scattered spectrum. We are concerned only with the shape of the central peak.

In Fig. 7 we consider the case in which $\Theta_e > \Theta_i$. Comparison with Fig. 1 shows that the effect of two temperatures can be much the same as that of collisions. The main difference appears to be that the width of the central feature is significantly greater in the two-temperature case. It is interesting to note that the peak occurs approximately at a frequency corresponding to an ion-acoustic frequency for ions at the electron temperature. In Fig. 7, for example, the peak is located closer to the position one might expect for a 10-eV thermal plasma. Except for the significant decrease in the scattering function in

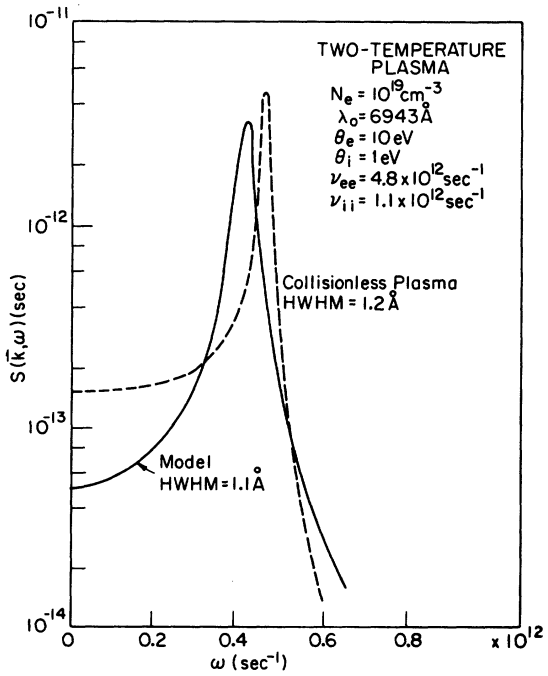

FIG. 7. Scattering function for a two-temperature plasma in which $\Theta_e > \Theta_i$.

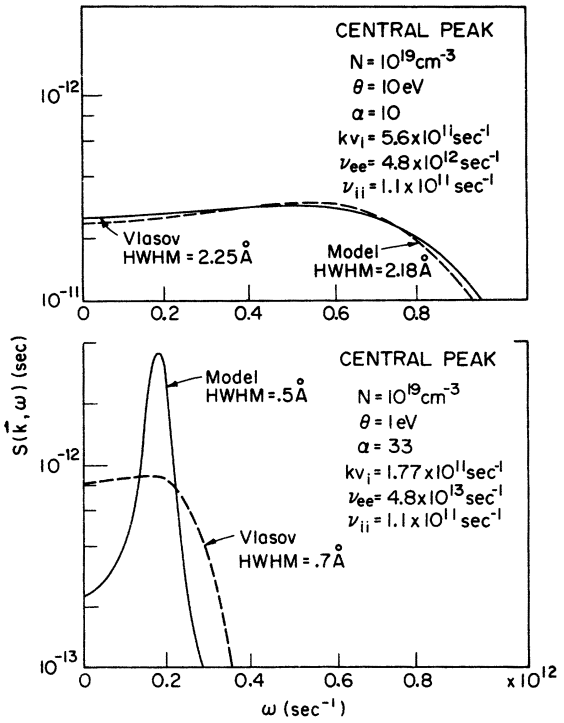

FIG. 8. Ion feature of the scattering function for plasmas in thermal equilibrium at 1 and 10 eV.

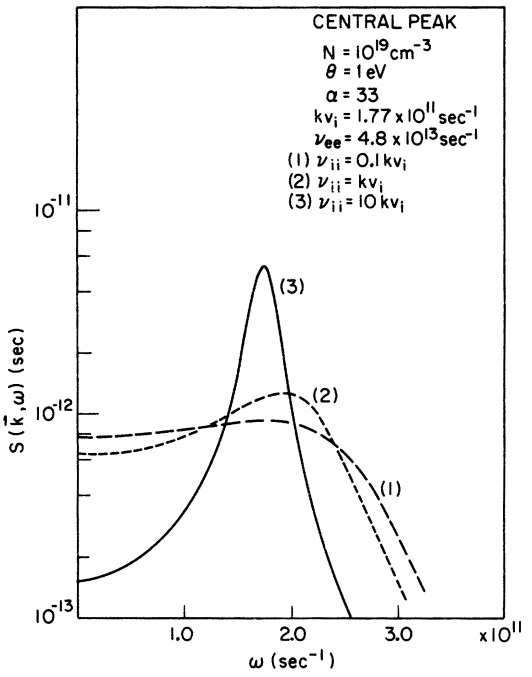

FIG. 9. Ion feature of the scattering function plotted for various values of ν_{ii}.

the region of zero frequency, collisions do not appear to have a very pronounced effect on the shape of the scattered spectrum in this case. For the case in which $\Theta_i = 10$ eV and $\Theta_e = 1$ eV, the effect of collisions is negligible.

Figure 8 illustrates the effect of collisions on the scattered spectrum of two thermal equilibrium plasmas which are identical except for temperature. It is clear as expected that the effect of collisions on the 1-eV plasma is markedly greater than the effect on the 10-eV plasma. Figure 8 should be kept in mind when analyzing the two-temperature case in Fig. 7.

5. *Effect of Varying the Collision Frequency*

The result of allowing the ion-ion collision frequency to vary independently of the other plasma parameters is illustrated for the central peak in Fig. 9 and for the satellite in Fig. 10. As the ion-ion collision frequency increases, there is an undamping of the ion-acoustic feature. This result is predicted by Bhadra and Varma[18] who compare the plasma ion sound wave to an ordinary sound wave propagating in a gas. In the case of very high molecular collision frequencies an ordinary sound wave is transmitted with practically no attenuation.[19] One can reason that the same effect is plausible for the plasma considered in Fig. 9

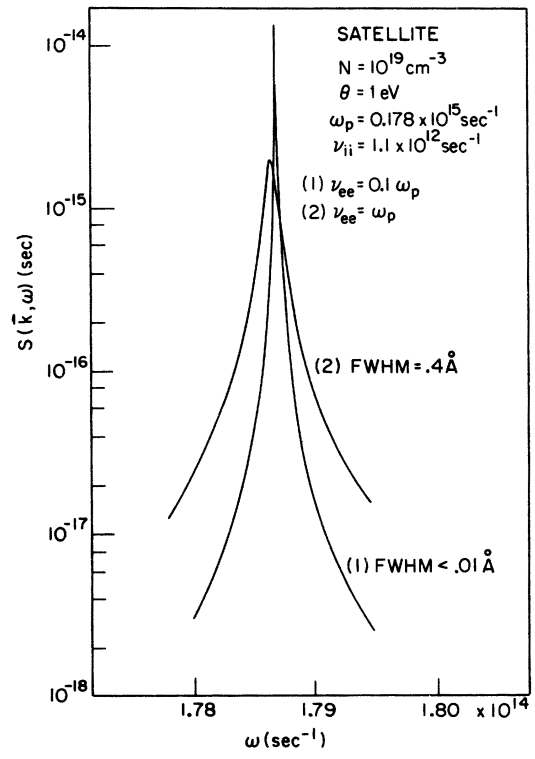

FIG. 10. Electron satellite feature of the scattering function $S(\vec{k}, \omega)$ plotted for various values of ν_{ee}.

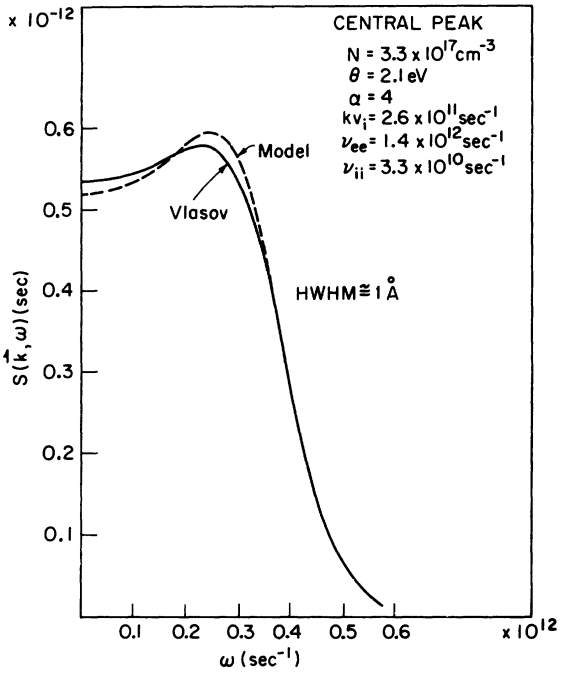

FIG. 11. Central peak of the scattering function plotted using the BGK collision model (dashed curve) and the collisionless model (solid curve).

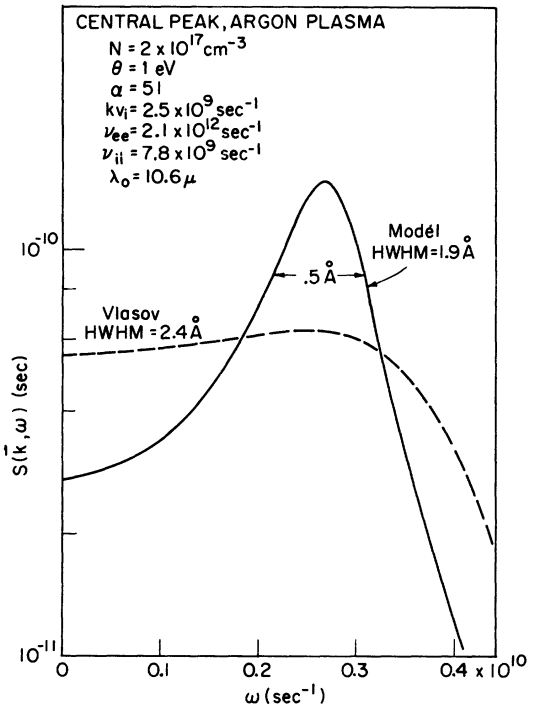

FIG. 12. Ion feature of the scattering function for CO_2 laser radiation (10.6 μ) scattered from an argon plasma.

owing to its high-density (comparable to gases at standard pressures) and collision-dominated nature.

Quite the opposite effect is observed on the satellite by varying the electron-electron collision frequency while holding the other parameters fixed. As is shown in Fig. 10, a higher collision frequency leads to more damping of the resonance at the plasma frequency. The actual collision frequency for the case shown in Fig. 10 lies between the values given for curves 1 and 2. Figs. 9 and 10 could be of more than just academic interest, if, for example, it were found that the collision frequencies were not adequately represented but that the remainder of the theory was quite good.

C. Comparison with Experiment

Comparison with existing experimental results is, on the whole, quite satisfactory. Most experiments to date have been done on plasmas in which collisional effects would not be expected to alter the shape of the scattered spectrum to any great extent.

The results of Ramsden and Davies[20] for a hydrogen plasma with a density of 2.4×10^{15} cm^{-3} and a temperature of 1 eV can be compared to our theoretical results in Figs. 2 and 4. For radiation scattered at 13.5°, corresponding to $\alpha = 3$, the resolution in the experiment was insufficient to determine anything other than the existence of the central peak and satellite. The theoretical result for the position of the satellite and the ratio of the intensity of the central peak to the satellite agree with the experimental observations.

A scattering experiment performed recently by Kato[21] demonstrated that the usual light-scattering theory gives valid experimental results even for plasmas with a small number of particles in a Debye sphere. He considered 90° scattering of ruby laser light from a hydrogen plasma with a density of 3.3×10^{17} cm^{-3} and a temperature of 1 eV. The number of particles in a Debye sphere for these conditions is 2. Figure 11 illustrates the effect of collisions on the scattered spectrum. Although the effect is quite noticeable, it is not experimentally resolvable in this case.

In the case of CO_2 (10.6-μ) scattering from an argon plasma, we are at odds with the experimental results reported by Offenberger and Kerr.[22] Figure 12 indicates some narrowing of the central peak and the usual enhancement of the ion-acoustic peak. In this case the scattered light is observed at an angle of 160°. The experimental results appear to reveal a central scattered linewidth of 0.5 Å whereas we obtain 3.8 Å. It should be noted that the width of the ion-acoustic peak is 0.5 Å,

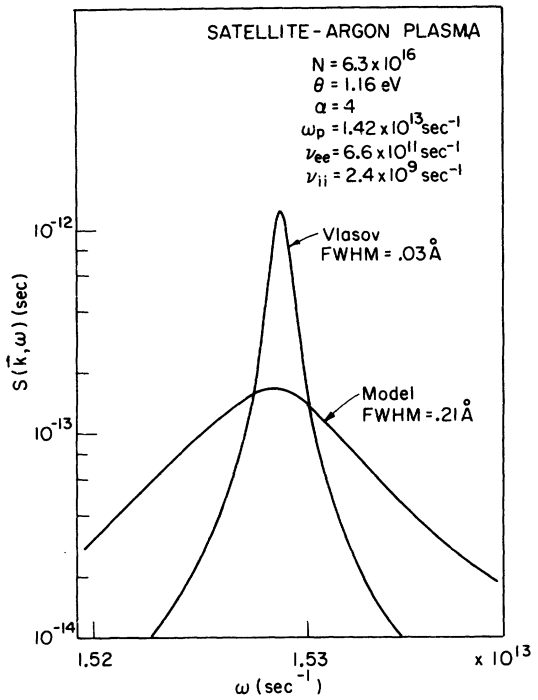

FIG. 13. Electron satellite feature of the scattering function for ruby laser light (6943 Å) scattered from an argon plasma.

but this peak is located 1.6 Å from the center.

The experimental parameters used by Chan and Nodwell[23] are incorporated into our theoretical formulation to give the curves shown in Fig. 13. In this case, ruby laser light is scattered from an argon plasma, and the scattering angle is 45°. The calculated satellites occur at a wavelength shift of approximately 39 Å in agreement with the experimental observations. The theoretical broadening due to collisions is quite pronounced. The experimentally observed linewidth is a good deal broader than the calculated linewidth. This is due mainly to density variations in the plasma which lead to the observation of a superposition of plasma lines at different frequencies.[23]

IV. CONCLUSION

This study was motivated by the desire to develop a method to account for binary collisions in a plasma in an external magnetic field. We were specifically interested in a method which would readily yield numerical results. We have employed a BGK model to account for collisions between like-charged particles. In the absence of an external magnetic field we obtain numerical results which agree well with experiments—where such experiments exist. Our results agree in the appropriate limits with those obtained using other models.

ACKNOWLEDGMENTS

The authors gratefully acknowledge assistance with the computer calculations from S. Karin, W. G. Price, L. Harding, and R. A. Jong. One of the authors (E.M.L.) was supported by an NDEA Title-IV Fellowship during part of this work.

APPENDIX

The density operator is defined as follows:

$$f_1^j(\vec{r},\vec{v},t)\equiv\sum_j \delta(\vec{r}-\vec{r}_j(t))\,\delta(\vec{v}-\vec{v}_j(t)), \tag{A1}$$

where $\delta(y)$ is the Dirac δ function. The vectors $\vec{r}_j(t)$ and $\vec{v}_j(t)$ denote the position and velocity in phase space of the jth particle at time t.

The density-fluctuation operator $\delta f^j(\vec{r},\vec{v},t)$ can now be defined

$$\delta f^j(\vec{r},\vec{v},t)\equiv f_1^j(\vec{r},\vec{v},t)-\langle f_1^j(\vec{r},\vec{v},t)\rangle. \tag{A2}$$

In the derivation of Eq. (3) the averaged density $\langle f_1^j(\vec{r},\vec{v},t)\rangle$, is taken to be a function of velocity only and is denoted by $f_0^j(v)$. The equations describing the density operator (see, for example, Ref. 14) are linearized using Eq. (A2). In this analysis an external magnetic field and binary collisions between charged particles are included in the formulation.

In the sense of certain approximations, the density-fluctuation operator is found to satisfy the linearized Boltzmann equation. The term $(\delta f^j/\delta t)_c$, generally found on the right-hand side of the Boltzmann equation and which represents the change in the distribution function owing to collisions within a Debye sphere, is represented in linearized form in Eq. (3) as follows:

$$\left.\frac{\delta f^j}{\delta t}\right|_c = I^{jj}\,\delta f^j + I^{kj}\,\delta f^j + I^{jk}\,\delta f^k. \tag{A3}$$

In Eq. (A3) self-collisions and cross collisions are considered separately.

---

*Work supported in part by the National Science Foundation under Grant No. GK-19360X.

†Based on a Ph.D. thesis by Ellen M. Leonard submitted to the Department of Nuclear Engineering, The University of Michigan.

[1]E. E. Salpeter, Phys. Rev. **120**, 1528 (1960).
[2]E. E. Salpeter, Phys. Rev. **122**, 1663 (1961).
[3]D. F. DuBois and V. Gilinsky, Phys. Rev. **133**, A1317 (1964).
[4]M. S. Grewal, Phys. Rev. **134**, A86 (1964).
[5]M. N. Rosenbluth and N. Rostoker, Phys. Fluids **5**, 776 (1962).

[6]J. P. Dougherty, Phys. Fluids **7**, 1788 (1964).
[7]C. S. Cheng and J. A. McLennan, Phys. Fluids **15**, 1285 (1972).
[8]P. L. Bhatnagar, E. P. Gross, and M. Krook, Phys. Rev. **94**, 511 (1954).
[9]S. Yip and M. Nelkin, Phys. Rev. **135**, A1241 (1964).
[10]J. P. Dougherty and D. T. Farley, Jr., J. Geophys. Res. **68**, 5473 (1963).
[11]W. R. Chappell and R. H. Williams, Phys. Fluids **14**, 1938 (1971).
[12]J. H. Williamson, R. A. Nodwell, and A. J. Barnard, J. Quant. Spectrosc. Radiat. Transfer **6**, 895 (1966).
[13]M. Lax, Rev. Mod. Phys. **32**, 25 (1960).
[14]R. K. Osborn, Phys. Fluids **11**, 595 (1968).
[15]Yu. L. Klimontovich, *The Statistical Theory of Non-Equilibrium Processes in a Plasma* (MIT Press, Cambridge, Mass., 1967), p. 125.
[16]Lyman Spitzer, Jr., *Physics of Fully Ionized Gases* (Interscience, New York, 1962).
[17]H. Röhr, Z. Phys. **209**, 295 (1968).
[18]D. Bhadra and R. K. Varma, Phys. Fluids **7**, 1091 (1964).
[19]G. E. Uhlenbeck and G. W. Ford, *Lectures in Statistical Mechanics* (American Mathematical Society, Providence, R. I., 1963).
[20]S. A. Ramsden and W. E. R. Davies, Phys. Rev. Lett. **16**, 303 (1966).
[21]M. Kato, Phys. Fluids **15**, 460 (1972).
[22]A. A. Offenberger and R. D. Kerr, Phys. Lett. A **37**, 435 (1971).
[23]P. W. Chan and R. A. Nodwell, Phys. Rev. Lett. **16**, 122 (1966).